Analyzing the errors of DFT approximations for compressed water systems

D. Alfè, A. P. Bartók, G. Csányi, and M. J. Gillan

Citation: The Journal of Chemical Physics **141**, 014104 (2014); doi: 10.1063/1.4885440
View online: http://dx.doi.org/10.1063/1.4885440
View Table of Contents: http://scitation.aip.org/content/aip/journal/jcp/141/1?ver=pdfcov
Published by the AIP Publishing

Analyzing the errors of DFT approximations for compressed water systems

D. Alfè,[1,2,3,4] A. P. Bartók,[5] G. Csányi,[5] and M. J. Gillan[2,3,4,a)]
[1]*Department of Earth Sciences, UCL, London WC1E 6BT, United Kingdom*
[2]*London Centre for Nanotechnology, UCL, London WC1H 0AH, United Kingdom*
[3]*Thomas Young Centre, UCL, London WC1H 0AH, United Kingdom*
[4]*Department of Physics and Astronomy, UCL, London WC1E 6BT, United Kingdom*
[5]*Department of Engineering, University of Cambridge, Cambridge CB2 1PZ, United Kingdom*

(Received 7 April 2014; accepted 16 June 2014; published online 2 July 2014)

We report an extensive study of the errors of density functional theory (DFT) approximations for compressed water systems. The approximations studied are based on the widely used PBE and BLYP exchange-correlation functionals, and we characterize their errors before and after correction for 1- and 2-body errors, the corrections being performed using the methods of Gaussian approximation potentials. The errors of the uncorrected and corrected approximations are investigated for two related types of water system: first, the compressed liquid at temperature 420 K and density 1.245 g/cm^3 where the experimental pressure is 15 kilobars; second, thermal samples of compressed water clusters from the trimer to the 27-mer. For the liquid, we report four first-principles molecular dynamics simulations, two generated with the uncorrected PBE and BLYP approximations and a further two with their 1- and 2-body corrected counterparts. The errors of the simulations are characterized by comparing with experimental data for the pressure, with neutron-diffraction data for the three radial distribution functions, and with quantum Monte Carlo (QMC) benchmarks for the energies of sets of configurations of the liquid in periodic boundary conditions. The DFT errors of the configuration samples of compressed water clusters are computed using QMC benchmarks. We find that the 2-body and beyond-2-body errors in the liquid are closely related to similar errors exhibited by the clusters. For both the liquid and the clusters, beyond-2-body errors of DFT make a substantial contribution to the overall errors, so that correction for 1- and 2-body errors does not suffice to give a satisfactory description. For BLYP, a recent representation of 3-body energies due to Medders, Babin, and Paesani [J. Chem. Theory Comput. **9**, 1103 (2013)] gives a reasonably good way of correcting for beyond-2-body errors, after which the remaining errors are typically 0.5 m$E_h \simeq 15$ meV/monomer for the liquid and the clusters. © *2014 AIP Publishing LLC*. [http://dx.doi.org/10.1063/1.4885440]

I. INTRODUCTION

The first-principles description of water systems based on density functional theory (DFT) remains unsatisfactory, despite efforts going back more than 20 years.[1,2] The problems of standard DFT approximations include erroneous energetics of water clusters,[3–9] incorrect relative energies and volumes of ice structures,[10–17] and poor predictions of the thermodynamic, structural, and dynamical properties of the liquid.[9,18–35] Water systems are made difficult by the subtle balance between low- and high-density structures seen in the cluster, ice, and liquid states.[17] The present work on the compressed liquid and clusters is motivated by the desire to deepen our understanding of this balance. We report simulations of the compressed liquid performed with both standard and corrected versions of DFT, comparing calculated thermodynamic and structural properties with experimental data, and using energy benchmarks from quantum Monte Carlo (QMC)[36–38] to help analyze the errors. We also use QMC and quantum-chemistry benchmarks on water clusters from the trimer to the 27-mer to investigate how DFT errors in the compressed liquid are related to those found in small finite systems.

Diffraction experiments show that liquid water undergoes major structural changes on compression.[39–44] The O–O radial distribution function (rdf) at ambient conditions indicates a structure related to that of ambient ice Ih,[45] with each monomer surrounded by ∼4 nearest neighbors at the typical hydrogen-bonding distance of ∼2.8 Å, second neighbors being at the much larger distance of ∼4.5 Å. On compression, the coordination number increases to values of at least 8 at ∼1 GPa (10 kilobars), and to 12 or more at ∼4 GPa. The experiments indicate that the changes result from close approach of monomer pairs that are not H-bonded to each other. These changes mirror the structural changes in compressed ice,[45] with the ambient-pressure forms ice Ih and ice XI being 4-fold coordinated and the compressed forms ice VII and VIII stable at pressures of between 1.5 and 60 GPa being 8-fold coordinated. Standard DFT approximations exaggerate the energy and pressure increases with increasing coordination number in ice,[13] and similar problems are expected in the compressed liquid. Here, we investigate how selected DFT approximations reproduce the experimentally known structure and thermodynamic properties of the liquid near the melting curve at the density for which the experimental pressure is 1.5 GPa.

a)Author to whom correspondence should be addressed. Electronic mail: m.gillan@ucl.ac.uk

Widely used DFT approximations such as PBE[46] and BLYP,[47] over-stabilize low-coordinated water structures relative to high-coordinated structures. This tendency is seen in the excessive differences between low- and high-density ice structures,[13] and also in the underestimated densities of the equilibrium liquid,[28,29,33–35] and the erroneous relative energies of isomers of the water hexamer.[4,8] Part of the problem lies in the incorrect description of dispersion interactions, and calculations on solid, liquid, and cluster forms of water have been reported using many varieties of dispersion-inclusive DFT.[4,6,13,16,27,29,30,33,35] However, these have met with only partial success, and the role of errors in other parts of the DFT energy, for example, polarization and exchange-repulsion interactions, is not yet clear.

We will make use of the exact many-body expansion (see, e.g., Refs. 7, 48, and 49), according to which the total energy $E_{\rm tot}(1, 2, \ldots N)$ of a system of N monomers is expressed as

$$E_{\rm tot}(1, 2, \ldots N) = \sum_i E^{(1)}(i) + \sum_{i<j} E^{(2)}(i, j) + E^{(>2)}(1, 2, \ldots N) . \quad (1)$$

Here $E^{(1)}(i)$ is the one-body (1B) energy of monomer i, $E^{(2)}(i, j)$ is the 2-body (2B) interaction energy of monomers i and j, and the beyond-2-body (B2B) energy $E^{(>2)}$ is everything not included in 1B and 2B energy. We and others have shown recently how this expansion can be used to analyze the errors of DFT not only for water clusters,[7,9,17,34] but also for ice structures[17,34] and for periodic configurations drawn from first-principles simulations of the liquid.[9] Analyses of this kind allow a separation of DFT errors into their 1B, 2B, and B2B components, thus giving further insight into the nature of these errors.

Our first-principles molecular dynamics (FPMD) simulations on the compressed liquid employ the BLYP and PBE approximations of DFT, and corrected versions denoted by BLYP-2 and PBE-2, which are constructed by elimination of 1B and 2B errors.[34] We choose to work with BLYP and PBE because these two approximations have been extensively used in previous first-principles work on water systems. The two approximations provide an instructive contrast, since their 2B errors differ greatly,[8] and their B2B errors are also very different.[9,17] Our techniques for eliminating the 1B and 2B errors of the BLYP and PBE approximations are based on the methods of Gaussian Approximation Potentials (GAP).[9,17,34,50] GAP is a rather general set of machine-learning methods, but here it provides a scheme for constructing accurate and systematically improvable representations of the differences between DFT and benchmark energies, the latter being obtained from wavefunction-based quantum chemistry. GAP correction for 1B and 2B errors implicitly includes correction for 2-body dispersion errors, as well as other types of 2-body error.

The present work makes extensive use of energy benchmarks from QMC.[36–38] The high accuracy of QMC for water systems is shown by recent work on ice structures and clusters,[8,13,51,52] which indicates that it is nearly as accurate as the "gold standard" CCSD(T) (coupled cluster with singles and doubles and perturbative triples) at the complete basis-set limit (see, e.g., Ref. 53). As we have shown,[9] the availability of QMC benchmarks for the total energy, in combination with GAP representations of the 1- and 2-body errors of DFT, permits calculation of the B2B errors of DFT for periodic "snapshots" of the liquid as well as thermally sampled configurations of large clusters. The strategy used here was used recently to analyze the B2B errors of BLYP in the ambient liquid.[9]

The large structural changes in liquid water induced by pressures of a few GPa were suggested by early simulations based on force-field models[54–56] and were confirmed by the neutron-diffraction work of Wu *et al.*[39] The dependence of liquid structure on pressure and temperature has since been studied in detail with x-ray diffraction[42–44,57] and neutron diffraction.[40,41,58] An important question has been whether the increase of coordination number from ∼4 to ∼12 over the pressure range 0–6 GPa implies disruption of the H-bonding network. Evidence that H-bonding remains largely intact has been inferred from the O–O, O–H, and H–H partial rdfs extracted from neutron diffraction measurements.[41] The earliest FPMD simulations of compressed liquid water[59] were performed beyond the pressure range where comparison with experiment could be made. Much subsequent FPMD work has focused on still higher pressures[60–66] where molecular dissociation is dominant, and is not directly relevant to the present work. Supercritical conditions[67] are also very different from those of interest here. The only previous FPMD simulations of the liquid that we know of at pressures of a few GPa near the melting curve are those of Ikeda *et al.*,[43] which employ the little-used exchange-correlation functional of Hamprecht *et al.*[68] The FPMD work of Kang *et al.*[69] at very high temperatures is also of some relevance, as is the very recent dispersion-corrected FPMD work of Corsetti *et al.*[35] on the compressibility of the near-ambient liquid.

The state having temperature $T = 420$ K and density 1.245 g/cm^3, corresponding to experimental pressure 1.5 GPa, was chosen for the present simulations because it was studied in the neutron diffraction work of Strässle *et al.*[41] and is close to states studied with x-ray diffraction by Weck *et al.*[42] After summarizing our techniques (Sec. II), we present our simulation results in Sec. III, where we test the uncorrected and corrected DFT approximations by comparing with thermodynamic and structural data from experiment and with energetic data from QMC. Use of the many-body expansion to separate 2B and B2B errors allows us to show the importance of B2B errors, as has been done for other water systems.[7–9,17,34] To gain further insight, we present (Sec. IV) results for these errors in thermal samples of compressed clusters ranging from the 3-mer to the 27-mer, using coupled-cluster and QMC benchmarks to compute these errors. An overall summary is given in Sec. VI.

II. TECHNIQUES

The VASP code[70] was used for all the FPMD simulations of the compressed liquid. The calculations employed the projector augmented wave (PAW) technique[71] with a plane-wave cut-off of 1200 eV and core radii of 0.8 bohr for H and 1.1 bohrs for O. The simulations were performed in the

(N, V, T) ensemble, with the Andersen thermostat[72] used to ensure canonical sampling. We implemented the thermostat by drawing new velocities from the appropriate Gaussian distribution at intervals of 0.1 ps. Since we are not concerned with dynamics here, we avoid the need for a very short time step by setting both the O and H masses to 16 amu, all our FPMD simulations being performed with the time step $\Delta t = 1.0$ fs. For details of equilibration times and lengths of production runs, see below (Sec. III A). Our DFT energy calculations on the clusters with PBE were done as for the liquid, but with the somewhat lower plane-wave cut-off of 875 eV. The BLYP calculations on the clusters were performed with the PWSCF code,[73] employing pseudopotentials of von Barth-Car and Troullier-Martins types for H and O, respectively, the plane-wave cut-off being 3400 eV.

Details of our GAP techniques for correcting 1B and 2B errors of any chosen DFT approximation are given in Ref. 34. The GAP corrections used in the present work employ the configuration sets and benchmarks described in Ref. 17, which provides examples demonstrating the high accuracy of the corrections. We denote by BLYP-1 and PBE-1 the approximations obtained by correcting BLYP and PBE for 1B errors alone, and by BLYP-2 and PBE-2 the approximations after correction for both 1B and 2B errors. Our FPMD simulations based on BLYP-2 and PBE-2 employ a modified version of the VASP code, with corrections to the forces and stress tensor being based on formulas for the exact derivatives of the GAP energy corrections.

The QMC benchmark energies for snapshots of the liquid in periodic boundary conditions and for all the clusters from 9-mer to 27-mer were performed by diffusion Monte Carlo (DMC)[36–38] with the CASINO code,[74] using the settings described in our previous work.[9] The same Dirac-Fock pseudopotentials[75] were used, non-locality being treated in the usual locality approximation. The trial wavefunctions were of Slater-Jastrow type, with a single Slater determinant, the single electron orbitals being obtained from DFT-LDA plane-wave calculations with the PWSCF package,[73] using the same plane-wave cut-off as before. The orbitals were represented in a basis of B-splines,[76] and the time step was 0.005 a.u. (For the tests justifying this choice of time step, see Refs. 9 and 13.)

Our calculations of benchmark values of the 3B energy of H_2O trimers (Sec. IV A) employ the CCSD(T) technique close to the complete basis-set limit, rather than QMC. These calculations were performed using the MOLPRO code.[77,78] The strategy used to ensure accurate basis-set convergence is described in an earlier report.[8] This involves the separation of the 3B energy into its Hartree-Fock and correlation parts, with the correlation part computed using the second-order Møller-Plesset (MP2) technique as an initial approximation. The difference between the CCSD(T) and MP2 correlation energies is then added as a final correction. Details of the counterpoise and explicit-correlation (F12) techniques used are exactly as in Ref. 8. We use the Dunning augmented correlation-consistent basis sets aug-cc-pVXZ,[79,80] with X the cardinality, referred to here simply as AVXZ. We know from previous work[8] that with AVTZ the residual basis-set error on the HF 3B energy and the MP2 correlation component of 3B energy is no more than $\sim 10\ \mu E_h$ (0.27 meV). For the δCCSD(T) correction to the correlation component of the 3B energy, we use AVDZ, which is expected to incur a basis-set error of no more than $20\ \mu E_h$ in the correction. For the DFT 3B energies, we use AVTZ, which leaves basis-set errors of no more than $\sim 10\ \mu E_h$.

We shall see that correction of BLYP and PBE for 1B and 2B errors still leaves significant errors in the energies of the liquid and the clusters and the pressure of the liquid. We recently showed[9] that a scheme due to Medders, Babin, and Paesani (MBP)[81,82] gives a useful way of correcting the B2B errors of BLYP for small clusters, and we use the same methods here. The scheme was described in detail in the original MBP paper[81] and our own implementation was outlined in the supplementary material of Ref. 9. Here, we recall the main points, and we explain how we have somewhat generalized the way of applying it.

We denote the benchmark 3B energy of an $(H_2O)_3$ cluster by $E^{(3)}_{\rm bench}(i, j, k)$ and the DFT approximation by $E^{(3)}_{\rm DFT}(i, j, k)$, both being functions of the positions, orientations, and internal deformations of monomers i, j, and k. We seek a function $\phi(i, j, k)$ which approximately represents the 3B errors:

$$\phi(i, j, k) \simeq \Delta E^{(3)}(i, j, k) \equiv E^{(3)}_{\rm DFT}(i, j, k) - E^{(3)}_{\rm bench}(i, j, k), \tag{2}$$

and we mitigate the B2B error of DFT for any water system by subtracting the sum $\sum_{i<j<k} \phi(i, j, k)$ of all its 3B errors. Following Ref. 81, $\phi(i, j, k)$ is the product of factors s_3 and V_3, with s_3 an overall smooth cut-off function and V_3 a sum of products of functions $\eta(r_{ab})$, with r_{ab} the distance between atoms a and b in different monomers. The function s_3 depends only on the three O–O distances and on inner and outer cut-off distances R_I and R_F, chosen to optimize the representation. Included in V_3 are products of two functions $\eta(r_{ab})\eta(r_{cd})$ and products of three functions $\eta(r_{ab})\eta(r_{cd})\eta(r_{ef})$, with the condition that in every such product there is at least one atom from every one of the three monomers. To ensure invariance of $\phi(i, j, k)$ under interchange of any two monomers and under interchange of the H atoms in any given monomer, we work with symmetrized sums of products $\kappa_n(i, j, k)$, where each κ_n is the sum of a chosen second-degree product $\eta(r_{ab})\eta(r_{cd})$ or third-degree product $\eta(r_{ab})\eta(r_{cd})\eta(r_{ef})$ and all the distinct products formed from it by permutation of monomers and intra-monomer interchange of H atoms (see Ref. 81 for details). The function V_3 is then represented as a linear combination $\sum_n c_n\kappa_n(i, j, k)$ of the "basis functions" κ_n. As in Ref. 81, the $\eta(r)$ are chosen to be decaying exponentials $\eta(r) = \exp(-kr)$, with k being adjustable inverse lengths, which differ for O–O, O–H, and H–H pairs.

In the original MBP scheme, the coefficients c_n are determined by a least-squares fit of $\phi(i, j, k)$ to the 3B error $\Delta E^{(3)}(i, j, k)$ for a large set of trimer configurations. However, this places only weak constraints on the cut-off function s_3, which is crucially important for extended water systems. In this work, we therefore prefer to perform a "global" least-squares fit of $\phi(i, j, k)$ to a large set of configurations of clusters of different sizes and of the periodic liquid, as well as trimers. Naturally, this approach can work only if the

B2B errors of the systems involved in the fit are mainly 3B errors.

III. COMPRESSED LIQUID

Our calculations on the liquid at $T = 420$ K and density (light water, H_2O) 1.245 g/cm^3 (1245 kg m^{-3}) are of two kinds. First, we report FPMD simulations based on BLYP and PBE and their corrected versions BLYP-2 and PBE-2 (see Sec. II). These simulations used cubic cells with 64 monomers per cell, the cube edge being $L = 9.1638$ Å. The second kind of calculation consists of energy benchmarks from diffusion Monte Carlo on samples of configurations drawn from DFT simulations of the liquid performed on 32-monomer periodic systems. Systems of only 32 monomers would give inaccurate thermodynamic and structural quantities, but our earlier tests[9] indicate that such systems suffice to assess the *differences* between DFT and QMC energies. The liquid configurations used for our QMC benchmarks come from FPMD simulations performed with BLYP, PBE, and their corrected counterparts.

A. First-principles molecular dynamics simulations

Our FPMD simulations had a duration of typically 40 ps, of which the first 10 ps were discarded for equilibration (see Table I). The equilibration time was decided by monitoring the evolution of the energy (recall that these are constant-T simulations) in sub-periods of the simulation. The average pressures computed from the production parts of the simulations are compared in Table I with experimental values at the given temperature and density. We report both the raw values of pressure computed directly from the simulations and the values after correction for two kinds of systematic error: First, our earlier tests[9] on simulations at ambient conditions indicate that with our chosen plane-wave cut-off a Pulay correction of ∼0.2 GPa (2 kilobars) is needed; second, previous work[29] suggests that simulations of liquid water with 64 monomers overestimate the pressure by ∼0.1 GPa compared with the thermodynamic limit. The net correction to be added to our raw values is thus 0.1 GPa. The computed internal energies given in the table for each DFT approximation do not include the kinetic energy of the nuclei, and are relative to the energy of isolated water molecules computed with the same DFT approximation, always at the standard equilibrium geometry of Partridge and Schwenke.[83] We do not attempt a comparison with the experimental internal energy of the liquid relative to the vapor, because this quantity is expected to be strongly affected by quantum nuclear effects. (Infrared data[84] indicate that the molecular stretch frequencies are lowered by something like 10% relative to the free molecule, and the resulting loss of zero-point energy would be expected to stabilize the liquid by around 2 mE_h (∼50 meV) per monomer.) However, the errors on the DFT energies will be quantified below using benchmarks from QMC.

TABLE I. Duration of FPMD simulations, excluding equilibration period, and computed time average of pressure and internal energy, with energy relative to that of isolated H_2O monomer at equilibrium geometry of Partridge and Schwenke.[83] Values of pressure in parentheses are obtained by correction for errors of plane-wave cut-off and finite cell size. (Units: 1 GPa = 10 kilobars; 1 mE_h = 27.2 meV = 0.63 kcal/mol.)

Method	Duration (ps)	Pressure (GPa)	Energy (mE_h/monomer)
BLYP	20	3.14 (3.24)	− 6.7
PBE	33	2.25 (2.35)	− 11.5
BLYP-2	34	1.13 (1.23)	− 14.1
PBE-2	23	2.22 (2.32)	− 10.3
Expt.	...	1.50	...

The computed pressures show substantial errors. The BLYP and PBE pressures are too high by factors of 2.2 and 1.6, respectively, and correction of PBE for its 1B and 2B errors makes little difference. The BLYP-2 pressure is too low by 18%. The excessive pressures with BLYP and PBE are expected, since earlier work[29] shows that at ambient density BLYP and PBE give pressures that are too high by ∼0.7 GPa and 0.4 GPa, respectively. The failure of PBE-2 to improve the pressure indicates that the problem is not due to a poor description of dispersion, which should be mainly a 2B effect. The unreliability of the computed internal energies is also clear. The difference of binding energy by over a factor of 2 between BLYP and BLYP-2 is not a surprise, since earlier work on liquid water and ice[9,17,34] shows that BLYP and BLYP-2 will be underbound and overbound, respectively.

We noted in the Introduction the qualitative change of structure revealed by diffraction experiments[39–44] as pressure is increased from ambient to around 1 GPa. This change is clear from a comparison of the O–O rdf given by our present high-pressure BLYP-2 simulation with our recent ambient-pressure BLYP-2 simulation at $T = 350$ K,[9] shown in Fig. 1. In agreement with x-ray and neutron experiments, the position of the first peak remains almost unchanged, while the second peak at ∼4.2 Å suffers complete collapse, with the second neighbors moving inward to form a broad shoulder on the first peak.

Comparison of the partial rdfs $g_{\alpha\beta}(r)$ from our four FPMD simulations with the neutron diffraction results of

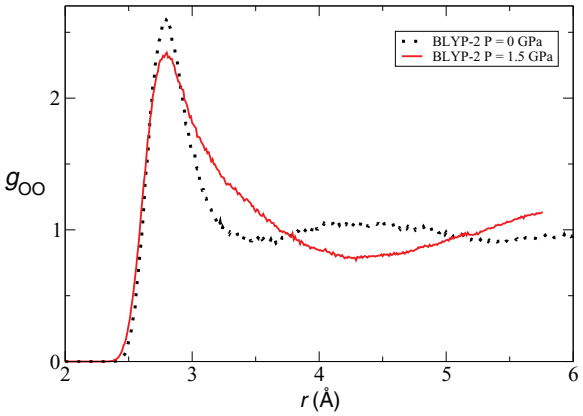

FIG. 1. Comparison of O–O radial distribution functions $g_{OO}(r)$ from simulations performed with BLYP-2 approximation at high pressure (red solid curve) and near-ambient pressure (black dotted curve). High-pressure $g_{OO}(r)$ is from present work at $T = 420$ K and density $\rho = 1.245$ g/cm^3 (1245 kg m^{-3}), low-pressure $g_{OO}(r)$ is from BLYP-2 simulation reported in Ref. 9 at $T = 350$ K, $\rho = 1.049$ g/cm^{-3}.

Strässle *et al.*[41] at $P = 1.5$ GPa, $T = 420$ K (Fig. 2) shows reasonable overall agreement, though there are some significant differences between the simulation rdfs. The predictions of PBE-2 and BLYP-2 are very close to each other, but differ noticeably from those of PBE and BLYP. There are significant differences between the approximations for $g_{OO}(r)$, with more inward displacement of the second shell into the region of the first shell with BLYP-2 and PBE-2 and considerably less with PBE. The differences between the approximations for $g_{OH}(r)$ are also significant, with BLYP-2 and PBE-2 showing appreciably less structure than BLYP and PBE. We note that the first peak in $g_{OO}(r)$ from simulation is slightly lower and broader and displaced to high r compared with experiment, except in the case of PBE, but the position of the first minimum is very poor with PBE. A striking deviation from experiment is the greater structuring of $g_{OH}(r)$ around the first minimum and second maximum produced by all the simulations. Many authors have shown[82,85–87] that quantum nuclear effects significantly soften the structure of liquid water, and the softening is particularly marked for g_{OH} and g_{HH}. These effects may partly explain the differences between simulation and experiment.

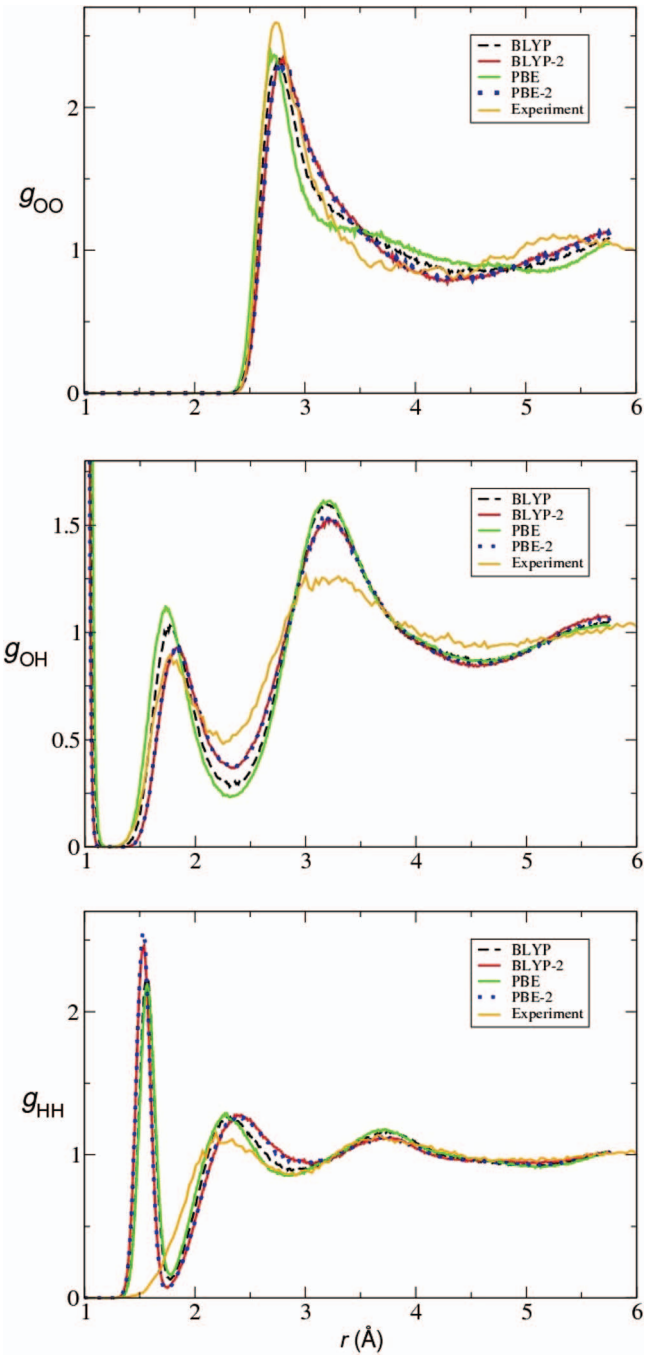

FIG. 2. Comparison of O–O, O–H, and H–H radial distribution functions $g_{\alpha\beta}(r)$ from present FPMD simulations with neutron-diffraction measurements of Strässle *et al.*[41] FPMD results are from simulations performed with BLYP (black dashed), BLYP-2 (red solid), PBE (green solid), and PBE-2 (blue dotted) approximations, with experimental results shown as yellow solid curves. Note: intra-molecular O–H and H–H peaks are excluded from experimental results.

In assessing the discrepancies between our simulations and neutron diffraction, we note that the extraction of the three $g_{\alpha,\beta}(r)$ from the experiments does not employ isotope substitution,[40,88] but instead uses the EPSR technique (empirical potential structure refinement).[89] In this approach, the measured structure factor $S(q)$ is compared with the structure factor predicted by molecular dynamics simulations based on a standard reference potential (the SPC/E model[90] was used by Strässle *et al.*[41]) together with a superimposed empirical potential. The latter potential is then refined to fit the measured $S(q)$. However, we can avoid any uncertainties arising from the EPSR procedure itself by directly computing $S(q)$ from our simulations. The required formulae are given in standard references, e.g., Ref. 91. Since the neutron diffraction measurements of Strässle *et al.* were performed on D_2O, we use the coherent neutron scattering lengths of ^{16}O and ^{2}H.

In Fig. 3, we compare the $S(q)$ from our BLYP-2 simulation with experimental data and the EPSR fit. The overall agreement for wavevectors $1.7 < q < 15.0$ Å^{-1} is good (upper panel), but there are significant discrepancies in the region $2.5 < q < 6.0$ Å^{-1} (see lower panel). Specifically, there is a systematic offset between the BLYP-2 $S(q)$ on the one hand and the experimental and EPSR $S(q)$ on the other hand between 4.5 and 6.0 Å^{-1}. The difference is small, but this q region appears to be important, because Strässle *et al.*[41] show that this is where the measured $S(q)$ depends most strongly on thermodynamic state. Most of the differences visible in Fig. 2 appear to arise from small differences in this region. It is natural to ask whether the neutron diffraction data contain enough information to distinguish between the structures predicted by our four DFT approximations. We have tested this by comparing the $S(q)$ produced by BLYP-2, PBE and BLYP simulations with the experimental data. The comparisons (see supplementary material[92]) show significant differences in the region around 4.4 Å^{-1}, where PBE and BLYP display a pronounced peak, which is weak with BLYP-2 and absent from experiment. All the simulations show the systematic offset from experiment for $4.5 < q < 6.0$ Å^{-1}. In addition, PBE and BLYP deviate significantly from experiment around $q \sim 3.0$ Å^{-1}. Thus none of the DFT approximations agrees perfectly with experiment, but BLYP-2 and PBE-2 agree better than PBE and BLYP.

We have analyzed the close approach of non-H-bonded neighbors by separating the O–O rdf into H-bonded and non-H-bonded contributions $g_{OO}^{HB}(r)$ and $g_{OO}^{NHB}(r)$. Following Luzar

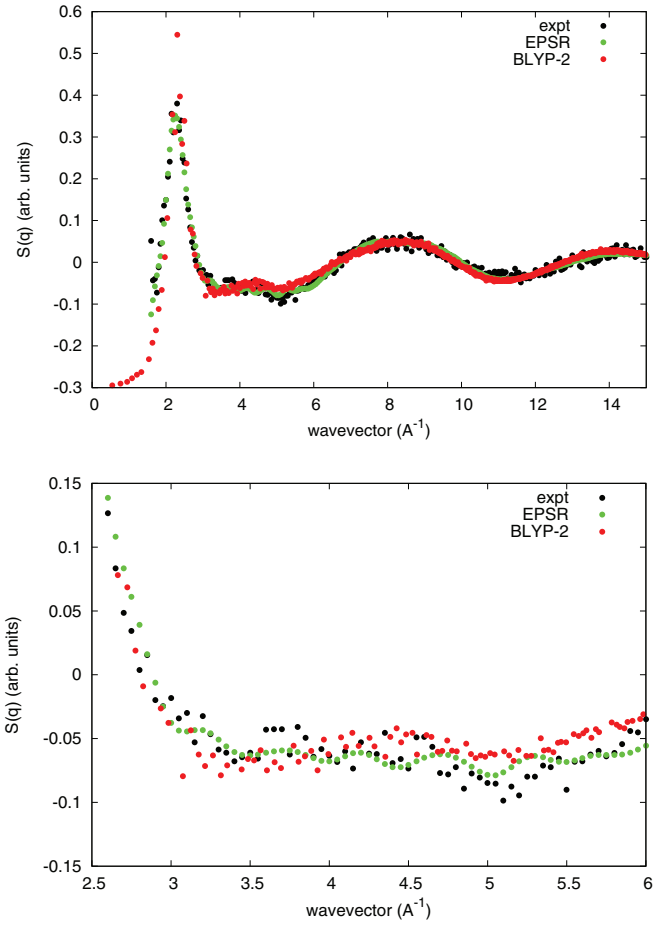

FIG. 3. Neutron-weighted structure factor $S(q)$ (see text) computed from present BLYP-2 simulations of liquid water at $T = 420$ K, $\rho = 1245$ kg m^{-1} (red points), compared with experimental measurements of Strässle *et al.*[41] (black points) and EPSR fit to experiment (green points). Lower panel shows expanded view of upper panel for restricted wavevector range $2.5 < q < 6.0$ Å^{-1}.

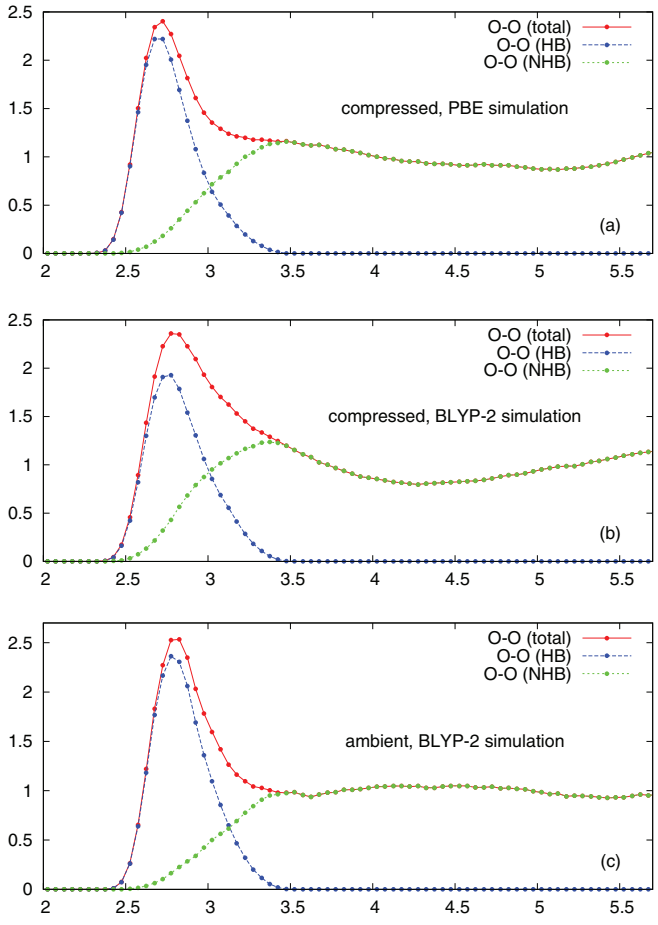

FIG. 4. Hydrogen-bonded and non-hydrogen-bonded components $g_{OO}^{HB}(r)$ and $g_{OO}^{NHB}(r)$ of the O–O radial distribution function $g_{OO}(r)$ from FPMD simulations of compressed liquid water ($T = 420$ K, $\rho = 1.245$ g/cm^3 $= 1245$ kg m^{-3}) with PBE and BLYP-2 approximations and near-ambient liquid water ($T = 350$ K, $\rho = 1.049$ g/cm^{-3}) with BLYP-2 approximation.

and Chandler,[93] we characterize the geometry of a monomer pair by the O–O distance r_{OO} and the four angles $\phi_{OH.O}$ between the intramolecular OH bonds and the intermolecular O–O axis. (The angles are such that if an H atom is between two O atoms, then $\phi_{OH.O}$ is zero.) A pair is counted as H-bonded if r_{OO} and $\phi_{OH.O}$ fall below chosen cut-off values. We define a H-bond weight w_{HB} as a product of distance and angle factors: $w_{HB} \equiv w_{HB}^r w_{HB}^\phi$. Here, w_{HB}^r is zero if $r_{OO} > r_1$ and is unity if $r_{OO} < r_0$, with r_0 and r_1 inner and outer cut-off distances; between r_0 and r_1 it is given by a smoothly connecting cubic function. Similarly w_{HB}^ϕ is zero and unity for $\phi_{min} > \phi_1$ and $\phi_{min} < \phi_0$ with smoothly connecting values between ϕ_0 and ϕ_1, ϕ_{min} being the smallest of the four angles $\phi_{OH.O}$. We then define the H-bonded component $g_{OO}^{HB}(r)$ of the O–O rdf exactly like the usual rdf $g_{OO}(r)$, except that contributions are weighted by w_{HB}; its non-H-bonded component is $g_{OO}^{NHB} \equiv g_{OO}(r) - g_{OO}^{HB}(r)$. We use inner and outer cut-off values r_0, $r_1 = 3.1$, 3.5 Å, and ϕ_0, $\phi_1 = 30°$, 40°.

We show in Fig. 4 the decomposition of $g_{OO}(r)$ into its HB and NHB parts for the PBE and the BLYP-2 simulations. (The BLYP results are intermediate between PBE and BLYP-2, and the PBE-2 results are almost the same as those from BLYP-2.) For comparison, we show the same decomposition from our recently reported BLYP-2 simulation of the liquid at ambient pressure and $T = 350$ K. These plots allow us to gauge the amount of penetration of NHB neighbors into the first shell of HB neighbors. According to the BLYP-2 simulations, there is significant penetration even at ambient pressure, with an appreciable probability of finding NHB monomers at the typical O–O distance of 2.8 Å characteristic of H-bonding. At 1.5 GPa (15 kilobars), BLYP-2 gives substantially increased penetration. The amount of penetration given by PBE and BLYP is very much less, and indeed the penetration with PBE at 1.5 GPa is no greater than with BLYP-2 at ambient pressure.

We asked in the Introduction whether the close approach of NHB monomers entails a disruption of the H-bonded network. The number of other monomers with which a monomer forms H-bonds is the sum of the weights w_{HB} between the given monomer and its neighbours, i.e., the integrated coordination number of $g_{OO}^{HB}(r)$. In our high-pressure simulations with BLYP, PBE, BLYP-2 and PBE-2, we find HB coordination numbers of 3.70, 3.77, 3.60, and 3.62. For comparison, the same analysis performed for our BLYP-2 simulation at ambient pressure yields the value 3.54. Similar numerical estimates of the number of H-bonds formed by each monomer

in ambient water have been reported by other researchers.[94] These comparisons indicate that the H-bonding network is not disrupted by compression.

B. Analysis of DFT errors using QMC benchmarks

We saw in Sec. III A that our DFT-based approximations predict very different internal energies, some of which must be seriously in error. However, detailed comparison with the experimental internal energy is difficult, since our FPMD simulations do not account for quantum nuclear effects. Here, we present QMC benchmark energies for sets of snapshots of the entire simulated system drawn from FPMD simulations. The high accuracy of QMC for water systems[8,13,51,52] allows us to quantify the energy errors of DFT for the liquid without any uncertainty from quantum nuclear effects. In addition, we obtain not only the thermal average of the errors, but also information about their fluctuations.

We have performed FPMD simulations on the 32-monomer liquid at the same compressed state as before, using the BLYP, PBE, BLYP-2, and PBE-2 energy functions. In these simulations, the equilibration time was typically 10 ps, and we drew 20 configurations at intervals of typically 1 ps from the subsequent production runs of each simulation, so as to form an overall sample of 80 configurations spanning the different kinds of structure represented by the rdfs of Fig. 2. We then calculated benchmark energies of these 80 configurations using DMC, and we also calculated their energies using BLYP, PBE, BLYP-2, and PBE-2.

By averaging over the 20 configurations drawn from each of the four simulations, we have computed the mean error per monomer and the rms fluctuation of this error for the four energy algorithms (Table II). With $E_{\rm DFT}$ the energy of a given DFT algorithm, and $E_{\rm DMC}$ the DMC energy, the error is $\Delta E \equiv E_{\rm DFT} - E_{\rm DMC}$. The mean value $\langle \Delta E \rangle$ is proportional to the number $N_{\rm molec}$ of monomers, so that the mean error per monomer is $\langle \Delta E \rangle / N_{\rm molec}$. The fluctuation of the error is $\delta \Delta E \equiv \Delta E - \langle \Delta E \rangle$, and we expect $\langle (\delta \Delta E)^2 \rangle$ to be proportional to $N_{\rm molec}$, so the rms reported in the table is $[\langle (\delta \Delta E)^2 \rangle / N_{\rm molec}]^{1/2}$.

TABLE II. Normalized mean errors $\langle \Delta E \rangle / N_{\rm molec}$ and root-mean-square fluctuations of errors $[\langle (\delta \Delta E)^2 \rangle / N_{\rm molec}]^{1/2}$ of energies computed with algorithm X for configurations drawn from simulations performed with energy algorithm Y (rms fluctuations are given in parentheses). Errors are computed as deviations from QMC benchmarks: $\Delta E \equiv E_{\rm DFT} - E_{\rm DMC}$, with $\delta \Delta E \equiv \Delta E - \langle \Delta E \rangle$ the fluctuation of the error about its mean value, and $N_{\rm molec}$ the number of molecules in the system. Energy algorithms X consist of uncorrected PBE and BLYP functionals, and their versions corrected for 1-body errors (PBE-1, BLYP-1) and for both 1- and 2-body errors (PBE-2, BLYP-2). Energy units: m$E_{\rm h}$ (1 m$E_{\rm h}$ = 27.2 meV = 0.63 kcal/mol.)

	Simulation method *Y*			
Energy alg. *X*	PBE	PBE-2	BLYP	BLYP-2
PBE	0.38 (1.56)	1.68 (1.34)	0.56 (1.87)	1.52 (1.40)
PBE-1	1.69 (0.85)	2.25 (0.67)	1.86 (1.22)	2.19 (0.76)
PBE-2	1.45 (0.51)	1.48 (0.51)	1.49 (0.46)	1.49 (0.41)
BLYP	4.89 (1.20)	5.92 (1.18)	4.99 (1.54)	5.79 (1.03)
BLYP-1	6.42 (0.58)	6.58 (0.57)	6.51 (0.80)	6.57 (0.51)
BLYP-2	− 2.52 (0.57)	− 2.38 (0.55)	− 2.42 (0.58)	− 2.39 (0.51)

Table II shows that uncorrected BLYP and its corrected version BLYP-1 are always severely underbound, by ∼5.5 and ∼6.5 m$E_{\rm h}$, respectively, while PBE and PBE-1 are always somewhat underbound, by ∼1.0 and ∼2.0 m$E_{\rm h}$, respectively (1 m$E_{\rm h}$ ≃ 27 meV ≃ 0.63 kcal/mol). The raising of energy caused by 1B corrections is expected, since the energy cost of distorting the H_2O monomer is too low with both BLYP and PBE.[8,95] Correction for 2-body errors gives substantial improvements, particularly for BLYP, but the resulting errors of ∼−2.5 and ∼1.5 m$E_{\rm h}$/monomer are still appreciable. (For comparison, the energy difference between 4-fold coordinated ice Ih and 8-fold coordinated ice VIII is only 1.2 m$E_{\rm h}$/monomer,[13,96] so errors of more than 1 m$E_{\rm h}$ must be considered important.) For all the configuration sets, the rms fluctuations of the errors always decrease monotonically as 1B and 2B errors are removed. The results of Table II will be highly relevant to our presentation of energy errors in thermal samples of water clusters in Sec. IV.

IV. THERMAL SAMPLES OF COMPRESSED CLUSTERS

In elucidating the relationship between DFT errors in the compressed liquid and in clusters, our main interest will be in beyond-2-body (B2B) errors, since we already know how to correct for 1B and 2B errors. We start by studying 3-body (3B) errors in a large sample of trimers chosen to represent the configurations found at both high and low pressures. We use this sample to show the usefulness of the MBP technique[81] for representing 3B energy errors. We then study the B2B errors of BLYP and PBE in samples of the 9-mer, the 15-mer, and the 27-mer clusters under compression. Our aim is to investigate how these errors evolve towards the errors found in the compressed liquid.

A. Three-body errors in compressed trimers

Our sample of trimer configurations is drawn mainly from our FPMD simulation of compressed liquid water performed with the BLYP-2 energy function (see Sec. III A), but also from an earlier simulation of the liquid at $T = 300$ K and zero pressure based on the empirical AMOEBA force field.[8] To extract trimers from the liquid, we take the atomic coordinates of the periodic system at a particular time step and repeatedly place a sphere of chosen radius $R_{\rm rad}$ at a random position until a case is found for which the number of monomers within the sphere is exactly 3. (For this purpose, a monomer is within the sphere if its O atom is within the sphere.) When such a case is found, the trimer in question is added to the list, and the procedure is repeated. The time-steps at which this is done are equally spaced at intervals of ∼0.1 ps. We formed a set of 230 configurations in this way with $R_{\rm rad} = 1.9$ Å. With $R_{\rm rad}$ this small, we find that the shortest O–O distance in each trimer is never greater than 3.0 Å and the longest is never greater than 3.7 Å, and in about 30% of cases all three distances are less than 3.2 Å, so that the trimers are all rather compact. A further set of 263 more extended trimers was formed using $R_{\rm rad} = 2.3$ Å. We added a further set of 207 trimers from the ambient AMOEBA simulation, these being drawn completely

at random subject only to the condition that the largest O–O distance is less than 4.5 Å. The overall set thus contains 700 trimer configurations spanning a wide range of geometries.

We computed CCSD(T) benchmark values and BLYP and PBE values of the 3B energies of our sample of 700 trimers, using the methods and basis sets outlined in Sec. II. Plots of the DFT errors, i.e., the differences $E^{(3)}$(DFT) − $E^{(3)}$(bench) against the benchmark 3-body energy $E^{(3)}$(bench) (Fig. 5) show that the 3B errors of PBE are almost entirely positive, with values typically in the range 0.2–0.6 mE_h, while those of BLYP are mainly in the range −0.3 to 0.2 mE_h, being mainly negative when the 3-body energy itself is negative. It is not accidental that the signs of these errors are the same as the signs of the errors of PBE-2 and BLYP-2 in the liquid, as we shall see.

We have performed least-squares fits of the MBP analytic representation of the 3B errors (see Sec. II). We show in Fig. 5 the corrected error plots obtained when the inner and outer cut-off distances R_I and R_F have the values 3.5 and 4.5 Å and the inverse decay lengths k_{OO}, k_{OH}, and k_{HH} have the values 0.5, 2.0, and 1.0 Å^{-1}, respectively. We see that the MBP representation is effective, since it achieves a substantial reduction of the 3B errors.

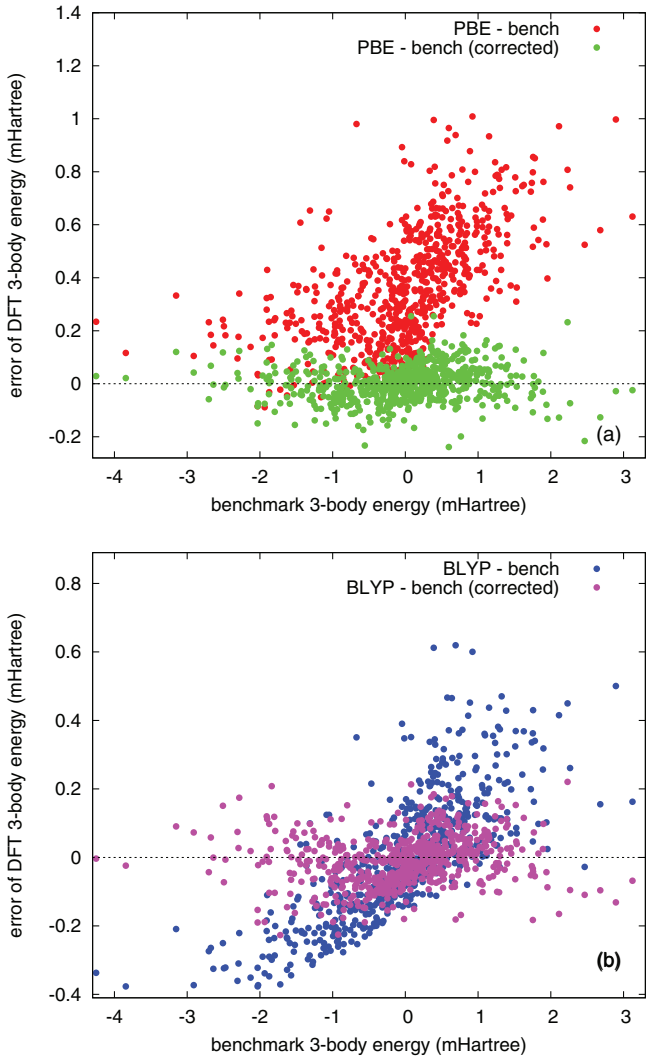

FIG. 5. Errors of PBE (upper panel) and BLYP (lower panel) approximations for 3-body energy of a sample of 700 configurations of the water trimer. Errors are computed as deviations from CCSD(T) benchmark values. For each approximation, errors are shown before (blue: BLYP, red: PBE) and after (magenta: BLYP, green: PBE) correction using the MBP scheme.[81] Units: mE_h.

B. Beyond-two-body errors in compressed nano-droplets

We generate sets of configurations that are roughly representative of water clusters in thermal equilibrium ("nano-droplets") following the method described in a previous report[9] This consists of running classical m.d. simulations using the TTM3-F model of Fanourgakis and Xantheas[85] (see Sec. II), with a weak confining potential added to suppress evaporation. For present purposes, we need to control the degree of compression of the cluster, which we characterize by the squared radius of gyration, defined by

$$R_{gyr}^2 = \frac{1}{N_{molec}} \sum_i |\mathbf{r}_i - \mathbf{r}_0|^2, \tag{3}$$

where $\mathbf{r}_i$ is the O position of monomer i, $\mathbf{r}_0$ is the centroid of the O positions of the entire cluster, and N_{molec} is the number of monomers in the cluster. During the simulation, R_{gyr} spontaneously fluctuates, but has a mean square value $\langle R_{gyr}^2 \rangle$ determined by the temperature and the force-field parameters. It is convenient to increase the compression, i.e., to reduce $\langle R_{gyr}^2 \rangle$, by making the dispersion coefficient C more negative. (The standard value of C in the model is $C = -723$ kcal/mol Å^6; note that 1 kcal/mol = 43.4 meV = 1.59 mE_h.)

Previously,[9] we computed DMC benchmarks for a set of 100 configurations each for the 9-mer and the 15-mer, of which 50 employed the standard value of C and the other 50 employed the reduced value −200 kcal/mol Å^6. Here, we generated a further 100 configurations each for the compressed 9-mer and 15-mer. Each set of 100 was assembled from subsets of 25 configurations drawn from separate TTM3-F simulations performed with $C = -1000$, -1500, -2000, and -2500 kcal/mol Å^6, these simulations being performed at $T = 200$, 250, 300, and 300 K and having a duration of typically 1 ns. We also present here DMC benchmarks for the 27-mer for a set of 100 configurations assembled from five subsets of 20 configurations drawn from separate TTM3-F simulations performed with $C = -1000$, -1250, -1500, -1750, and -2000 kcal/mol Å^6 at $T = 250$, 275, 300, 300, and 300 K.

The DMC benchmark energies for all configurations of the nano-droplets were computed in the usual way, the runs being long enough to reduce the statistical errors to ∼0.1 mE_h per monomer. The BLYP and PBE energies were computed in periodic boundary conditions with the PWSCF[73] and VASP[70] codes, respectively. The cube edge in all these calculations was chosen as 21.2 Å, on the basis of tests reported earlier.[9] GAP 1B and 2B corrections were then applied to obtain the BLYP-1, BLYP-2, PBE-1, and PBE-2 energies. We illustrate the results by showing (Fig. 6) the errors of the PBE-1, PBE-2, BLYP-1, and BLYP-2 energies (deviations from the DMC benchmarks) for the 100 configurations of the 27-mer

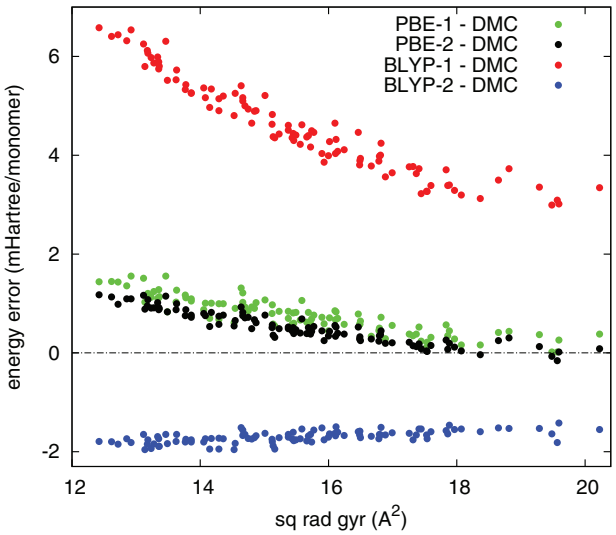

FIG. 6. Energy errors of binding energies of DFT-based approximations PBE-1, PBE-2, BLYP-1, and BLYP-2 for sample of 100 configurations of the water 27-mer cluster drawn from molecular dynamics simulations performed with the TTM3-F force-field (see text). Errors are plotted against squared radius of gyration of the cluster (see Eq. (3)). Units: mE_h/monomer.

nano-droplet, plotted against the squared radius of gyration. The errors for the 9-mer and the 15-mer (see the supplementary material[92]) are smaller, but have the same general form.

The plots for each approximation show a common pattern, revealing how the errors evolve with increasing cluster size. BLYP-1 is severely underbound, with errors that grow rapidly with increasing compression, making the cluster expand too much in thermal equilibrium. Correction for 2-body errors gives the overbound BLYP-2 approximation, whose B2B errors become more negative with compression, making the clusters contract too much. The sizes of the BLYP-1 and BLYP-2 errors grow with cluster size, reaching roughly 5 mE_h/monomer and -2 mE_h/monomer for the 27-mer, which are close to their counterparts in the liquid (see Table II). We have noted[9] that the dependence of the BLYP-1 and BLYP-2 errors on R^2_{gyr} is related to the errors in equilibrium density of the ambient liquid. The errors of PBE-1 and PBE-2 differ greatly from those of BLYP-1 and BLYP-2, and for the 9-mer are rather small. However, they grow with cluster size to nearly 2 mE_h/monomer for the compressed 27-mer, which is similar to their values in the compressed liquid (Table II). They increase with compression, as expected from the marked

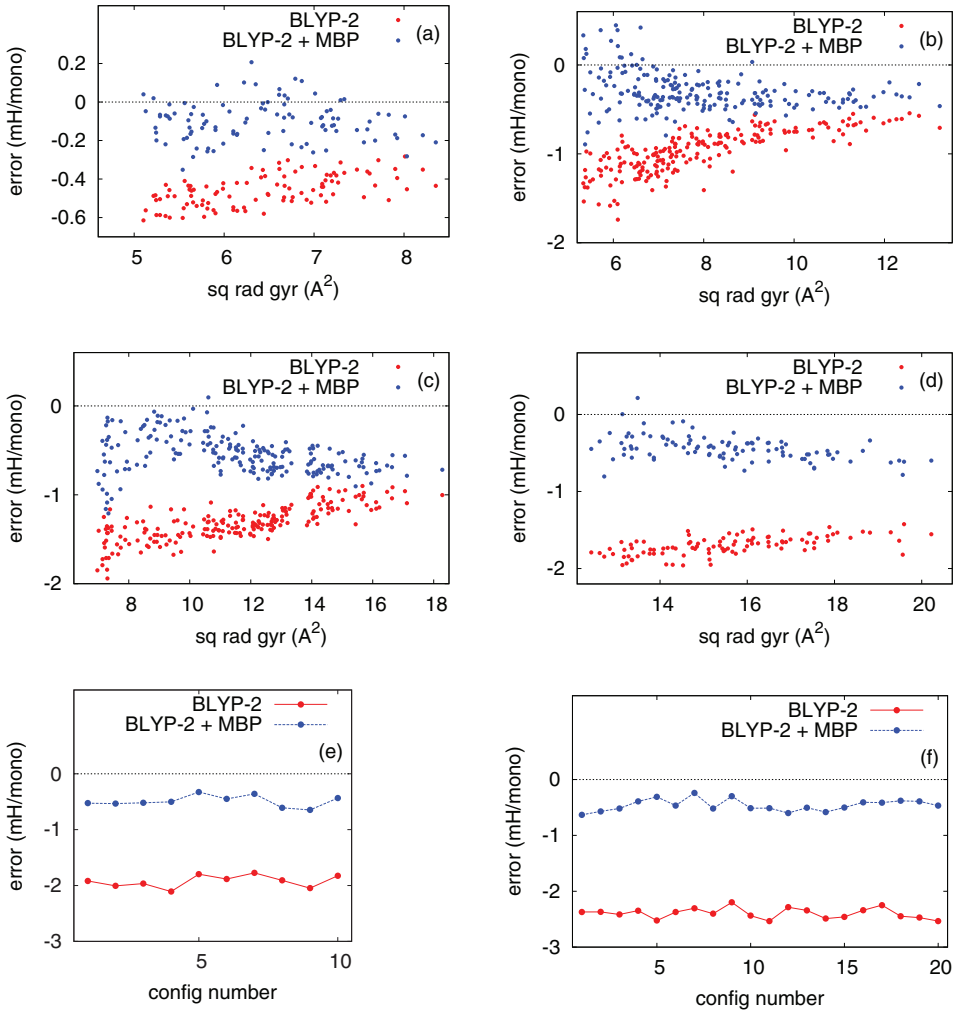

FIG. 7. Energy errors of BLYP-2 approximation before (red) and after (blue) MBP 3-body corrections. Upper four panels show errors for thermal samples of (a) 6-mer, (b) 9-mer, (c) 15-mer, and (d) 27-mer as function of squared radius of gyration R^2_{gyr} (see text). Lower two panels show errors for (e) 10 configurations of liquid at $\rho = 1.049$ g/cm^3, $T = 350$ K and (f) 20 configurations of compressed liquid at $\rho = 1.245$ g/cm^3, $T = 420$ K, both configuration sets being drawn from FPMD simulations based on the BLYP-2 approximation. Energy units: mE_h/monomer.

overestimation of pressure in the liquid with both PBE and PBE-2 (Table I). Importantly, the errors of PBE-2 in the clusters are only slightly less than those of PBE-1, so that they must be mainly B2B errors.

V. CORRECTING FOR BEYOND-TWO-BODY ERRORS

Our results for DFT errors in the nano-droplets suggest their close relationship with the corresponding errors in the liquid, and confirm the importance of B2B errors in both systems. The simplest scenario would be that the B2B errors are mainly 3B errors, in which case the representation of 3B errors presented in Sec. IV A could be used to correct the B2B errors of both clusters and liquid. We reported recently[9] that this method of correcting the B2B errors of BLYP-2 works well for clusters up to the 15-mer, but our initial attempts to extend this to the liquid were unsuccessful. One reason is that spatial cut-offs are very important for the liquid, but trimers alone do not give enough information about these cut-offs. However, we have had some success with an alternative strategy, in which the parameters of the MBP representation are determined by a "global" least-squares fit to the B2B errors of trimers, larger nano-droplets and liquid configurations, as described in Sec. II.

To show that this approach has merit, we compare in Fig. 7 the errors of BLYP-2 before and after correction using the global-fit MBP scheme for the 6-mer, 9-mer, 15-mer, and 27-mer nano-droplets and for configurations from our BLYP-2 simulations of both compressed and ambient liquid water. The DMC benchmarks and the BLYP-2 energies used here for the nano-droplets are taken from the results of Sec. IV B, while the corresponding results for the compressed liquid are for the 20 configurations from our BLYP-2 simulations (Sec. III). The data for the 6-mer and for the ambient liquid ($\rho = 1.049$ g/cm^3, $T = 350$ K) are taken from the work of Ref. 9. The cut-off distances R_I and R_F appearing in the function s_3 (see Sec. II and Ref. 81) have the values 3.5 and 4.5 Å respectively, and the inverse decay lengths k_{OO}, k_{OH}, and k_{HH} for O–O, O–H, and H–H pairs are 0.5, 2.0, and 1.0 Å^{-1}. The weights of the clusters and the liquid configurations in the least-squares fit were chosen to give a balanced representation of the B2B errors in the different systems. The results of Fig. 7 show that the correction of B2B errors using the MBP scheme achieves a considerable improvement, with the remaining errors after correction being typically $\sim$0.5 mE_h (15 meV) per monomer.

VI. DISCUSSION AND CONCLUSIONS

We have shown that the widely used BLYP and PBE approximations suffer from serious errors for compressed liquid water, even after correction for 1- and 2-body errors. This is at odds with the idea that the errors are mainly due to dispersion, which should be mainly a 2-body effect in water. Uncorrected BLYP underbinds the liquid with respect to free monomers by a factor of 2, while the BLYP-2 approximation obtained by correcting for 1B and 2B errors overbinds by 20% (errors of $\sim$5 m$E_h \simeq$ 140 eV/monomer and -2.5 m$E_h \simeq -65$ meV/monomer, respectively). The pressures with uncorrected and corrected BLYP are too high by a factor of 2 and too low by 25% (errors of 1.6 and -0.4 GPa), respectively. The errors of binding energy with uncorrected and corrected PBE are smaller (8% and 12%, or $\sim$1 mE_h $\simeq$ 30 meV/monomer and $\sim$1.5 m$E_h \simeq$ 40 meV/monomer, respectively), but the pressure errors are substantial (50% or 0.75 GPa both before and after correction). These errors are similar to well documented errors for the energetics of ice structures computed with PBE and BLYP and their 1- and 2-body-corrected counterparts.[13,16,17,34]

Comparison with diffraction data has been one of the key ways of testing DFT approximations, and very recently wavefunction-based methods, for ambient liquid water,[17,18,21,22,27–30,33,34,97] and we have presented a comparison of this kind for the compressed liquid. All our simulations reproduce semi-quantitatively the collapse of the second-neighbor shell in $g_{OO}(r)$ and the large increase of coordination number between ambient pressure and 1.5 GPa, but our simulated rdfs appear to differ significantly from those deduced from neutron diffraction[41]—in particular, our computed $g_{OH}(r)$ are appreciably more structured than the experimental data. The differences may be partly due to quantum nuclear effects, but we have also noted that the experimental rdfs were extracted from the measured structure factors $S(q)$ using the EPSR technique, and we have tested our simulations more directly against experiment by computing the neutron-weighted $S(q)$ from our simulations. The agreement between the $S(q)$ from experiment and simulation is good, but there are discrepancies that appear to be real, with the $S(q)$ from BLYP-2 and PBE-2 being better than the uncorrected versions.

The O–O rdfs from the various DFT approximations differ significantly. The $g_{OO}(r)$ from PBE, and to a lesser extent BLYP, show a less complete collapse of the second shell and a more extended shoulder on the first peak compared with the $g_{OO}(r)$ from BLYP-2 and PBE-2, which are almost identical to each other. The forms of these O–O rdfs suggest that BLYP-2 and PBE-2 make the close approach of non-H-bonded pairs more favorable than BLYP and PBE. We confirmed this by analyzing $g_{OO}(r)$ into H-bonded and non-H-bonded components. The analysis reveals substantial differences in the degree of penetration of non-H-bonded second neighbors into the shell of H-bonded first neighbors, with BLYP-2 and PBE-2 showing considerably more penetration than BLYP and particularly PBE. This same analysis confirms earlier indications from experiment[41] that the large change of structure caused by increasing pressure involves no disruption of the H-bonded network.

Our many-body analysis of DFT errors in thermal samples of compressed water clusters confirmed the importance of B2B errors[7–9,17] and showed that essentially the same errors seen in the liquid are already exhibited by quite small clusters. We showed that PBE and BLYP, when applied to a large sample of trimers drawn mainly from our simulations of the compressed liquid, suffer from substantial 3B errors. For PBE, these are systematically positive and have a typical value of $\sim$0.4 mE_h (11 meV). To see that this is important, we note that in the ice VIII structure there are 12 trimers per monomer having all three O–O distances less than 3.5 Å, so that the error just mentioned would cause ice VIII to be

underbound relative to ice Ih by 4.8 mE_h (130 meV). We saw that the 3B errors of BLYP can be both negative and positive, so that their net effect depends on the system of interest, but their magnitude is again significant. We found that the 3B errors of both PBE and BLYP are quite accurately represented by the scheme developed by Medders, Babin, and Paesani (MBP)[81] for representing the 3B errors of parameterized force fields for water.

The aim of our study of DFT errors in the larger nano-droplets was to trace the evolution of these errors as we approach the bulk liquid through finite systems of increasing size. By referring to QMC benchmarks, we found a consistent pattern of 2B and B2B errors for both BLYP and PBE. The B2B errors of BLYP are systematically negative, and for the 27-mer they are quantitatively close to what we observe in the liquid (~ -1.8 mE_h/monomer for the 27-mer versus -2.3 mE_h for the liquid). The consistent trend to more positive BLYP errors and more negative BLYP-2 errors with increasing compression of the cluster accords with the over- and under-estimates of pressure by BLYP and BLYP-2 in the compressed liquid. An important finding for the PBE approximation is that the errors of PBE-1 and PBE-2 are almost the same. The trend towards more positive errors with increasing compression in this case accords with the over-estimate of liquid pressure by both PBE and PBE-2.

Given the evident importance of B2B errors, we have sought ways of representing them that are valid for the entire range of systems we have studied—from trimers, through larger nano-droplets to the bulk liquid. We pointed out that this complex problem becomes manageable if we can assume that B2B errors are dominated by 3B errors. We showed that in this case a representation can be achieved by using the MBP scheme[81] to perform a "global" least-squares fit to the B2B errors of all the nano-droplets together with the bulk liquid. This idea turns out to work reasonably well for the B2B errors of BLYP-2, so that we then have a DFT approximation corrected for 1B, 2B, and B2B errors which represents the energies of the thermal samples for all the water systems treated here to within $\sim$0.5 m$E_h \simeq 15$ meV/monomer. Surprisingly, the same strategy does not appear to work well for the B2B errors of PBE-2, so that these errors are presumably not dominated by 3B contributions. The availability of a DFT approximation whose 1B, 2B, and B2B errors are well characterized and can be (mostly) corrected opens new opportunities, which we plan to explore. If our corrected BLYP total energy function is as good as our tests suggest, then it should be capable of reproducing the thermodynamic, structural, and dynamic properties of liquid water over a wide range of conditions. Finding out whether or not this is true will provide an important test of the ideas presented in this paper.

Whatever the fate of our corrected BLYP approximation, further analysis of the errors in existing DFT functionals is needed, even though exciting progress is beginning to be reported in the simulation of liquid water using correlated wavefunction-based methods.[97] An accurate description of dispersion is essential in water,[13,16,27–30,33,35] as it is in other molecular systems. However, dispersion is expected to be mainly a 2-body effect in water,[98] so that dispersion errors in water should be partly correctable by adding appropriate 2-body interaction potentials, as in the DFT+D schemes of Grimme.[99,100]) Since the GAP-based approach we use essentially eliminates all 2B (as well as 1B) errors, it automatically includes a correct description of dispersion, apart from many-body contributions. Although 3B (Axilrod-Teller-Muto) dispersion[101,102] is not entirely negligible in the ice VIII structure,[96] it cannot be responsible for the B2B errors of $\sim$2 mE_h/monomer that we have discussed here, so we should look elsewhere for the origin of these B2B errors. The sensitivity of 2B exchange-repulsion to the choice of exchange functional is well known,[103,104] and the effects can range from excessive repulsion (e.g., BLYP, revPBE) to spurious attraction (e.g. PW91).[104] Erroneous exchange can cause substantial 3B errors in rare-gas systems, where PBE is known to suffer from a positive 3B error.[105] Similar 3B errors have also been reported in the methane hydrate system.[106] The inaccurate description of polarizabilities by semi-local functionals is known to have a significant effect on the dielectric properties of water systems,[107] and this source of B2B errors could also be important. More detailed investigation of both kinds of B2B errors would therefore be timely.

In the course of this work and our other recent work, we have created a large data-base of QMC energy benchmarks for water systems ranging from small and large clusters to ice structures to periodic representations of the liquid under various conditions. We believe that this could serve as a useful resource in the development and testing both of improved density functionals and of parameterized force fields.[108] Until recently, accurate *ab initio* data was mainly confined to small clusters, but the availability of QMC calculations on both clusters and periodic systems, perhaps in combination with correlated quantum chemistry on periodic systems,[97] seems certain to change this situation for the better.[109,110]

In conclusion: (a) both uncorrected and corrected PBE and BLYP reproduce semi-quantitatively the large compression-induced changes of liquid structure given by diffraction experiments, and they confirm that compression does not disrupt the H-bonding network; (b) correction for 1- and 2-body errors causes significantly increased penetration of non-H-bonded neighbors into the shell of H-bonded first neighbors; (c) even after correction for these errors, the pressure and internal energy of the compressed liquid are poorly predicted, so that beyond-2-body errors are important; (d) the 2-body and beyond-2-body errors in the liquid are closely related to similar errors in compressed water clusters; (e) the beyond-2-body errors of BLYP can be quite well corrected by treating them as mainly 3-body errors.

ACKNOWLEDGMENTS

The project employed the resources of the Oak Ridge Leadership Computing Facility at ORNL, which is supported by the Office of Science of the DOE under Contract No. DE-AC05-00OR22725. A.P.B. was supported by a Junior Research Fellowship at Magdalene College Cambridge and by a Leverhulme Early Career Fellowship with joint funding from the Isaac Newton Trust. The authors thank T. Strässle

for providing numerical data from the experiments published in Ref. 41.

[1] K. Laasonen, M. Sprik, M. Parrinello, and R. Car, J. Chem. Phys. **99**, 9080 (1993).
[2] C. Lee, D. Vanderbilt, K. Laasonen, R. Car, and M. Parrinello, Phys. Rev. B **47**, 4863 (1993).
[3] J. A. Anderson and G. S. Tschumper, J. Phys. Chem. A **110**, 7268 (2006).
[4] B. Santra, A. Michaelides, M. Fuchs, A. Tkatchenko, C. Filippi, and M. Scheffler, J. Chem. Phys. **129**, 194111 (2008).
[5] E. E. Dahlke, R. M. Olson, H. R. Leverentz, and D. G. Truhlar, J. Phys. Chem. A **112**, 3976 (2008).
[6] A. K. Kelkkanen, B. I. Lundqvist, and J. K. Nørskov, J. Chem. Phys. **131**, 046102 (2009).
[7] F.-F. Wang, G. Jenness, W. A. Al-Saidi, and K. D. Jordan, J. Chem. Phys. **132**, 134303 (2010).
[8] M. J. Gillan, F. R. Manby, M. D. Towler, and D. Alfè, J. Chem. Phys. **136**, 244105 (2012).
[9] D. Alfè, A. P. Bartók, G. Csányi, and M. J. Gillan, J. Chem. Phys. **138**, 221102 (2013).
[10] D. R. Hamann, Phys. Rev. B **55**, R10157 (1997).
[11] P. Feibelman, Phys. Chem. Chem. Phys. **10**, 4688 (2008).
[12] I. Hamada, J. Chem. Phys. **133**, 214503 (2010).
[13] B. Santra, J. Klimeš, D. Alfè, A. Tkatchenko, B. Slater, A. Michaelides, R. Car, and M. Scheffler, Phys. Rev. Lett. **107**, 185701 (2011).
[14] O. Kambara, K. Takahashi, M. Hayashi, and J.-L. Kuo, Phys. Chem. Chem. Phys. **14**, 11484 (2012).
[15] Y. Fang, B. Xiao, J. Tao, J. Sun, and J. P. Perdew, Phys. Rev. B **87**, 214101 (2013).
[16] B. Santra, J. Klimeš, A. Tkatchenko, D. Alfè, B. Slater, A. Michaelides, R. Car, and M. Scheffler, J. Chem. Phys. **139**, 154702 (2013).
[17] M. J. Gillan, D. Alfè, A. P. Bartók, and G. Csányi, J. Chem. Phys. **139**, 244504 (2013).
[18] J. C. Grossman, E. Schwegler, E. W. Draeger, F. Gygi, and G. Galli, J. Chem. Phys. **120**, 300 (2004).
[19] M. Allesch, E. Schwegler, F. Gygi, and G. Galli, J. Chem. Phys. **120**, 5192 (2004).
[20] E. Schwegler, J. C. Grossman, F. Gygi, and G. Galli, J. Chem. Phys. **121**, 5400 (2004).
[21] P. H.-L. Sit and N. Marzari, J. Chem. Phys. **122**, 204510 (2005).
[22] H.-S. Lee and M. E. Tuckerman, J. Chem. Phys. **125**, 154507 (2006); **126**, 164501 (2007).
[23] M. Guidon, F. Schiffman, J. Hutter, and J. VandeVondele, J. Chem. Phys. **128**, 214104 (2008).
[24] T. D. Kühne, M. Krack, and M. Parrinello, J. Chem. Theory Comput. **5**, 235 (2009).
[25] S. Yoo, X. C. Zeng, and S. S. Xantheas, J. Chem. Phys. **130**, 221102 (2009).
[26] M. J. McGrath, I.-F. W. Kuo, and J. I. Siepmann, Phys. Chem. Chem. Phys. **13**, 19943 (2011).
[27] I.-C. Lin, A. P. Seitsonen, M. D. Coutinho-Neto, I. Tavernelli, and U. Röthlisberger, J. Phys. Chem. B **113**, 1127 (2009).
[28] J. Schmidt, J. VandeVondele, I.-F. W. Kuo, D. Sebastiani, J. I. Siepmann, J. Hutter, and C. J. Mundy, J. Phys. Chem. B **113**, 11959 (2009).
[29] J. Wang, G. Román-Pérez, J. M. Soler, E. Artacho, and M.-V. Fernández-Serra, J. Chem. Phys. **134**, 024516 (2011).
[30] A. Møgelhøj, A. Kelkkanen, K. T. Wikfeldt, J. Schiøtz, J. J. Mortensen, L. G. M. Pettersson, B. I. Lundqvist, K. W. Jacobsen, A. Nilsson, and J. K. Nørskov, J. Phys. Chem. B **115**, 14149 (2011).
[31] R. Jonchiere, A. P. Seitsonen, G. Ferlat, A. M. Saitta, and R. Vuilleumier, J. Chem. Phys. **135**, 154503 (2011).
[32] C. Zhang, J. Wu, G. Galli, and F. Gygi, J. Chem. Theory Comput. **7**, 3054 (2011).
[33] Z. Ma, Y. Zhang, and M. E. Tuckerman, J. Chem. Phys. **137**, 044506 (2012).
[34] A. P. Bartók, M. J. Gillan, F. R. Manby, and G. Csányi, Phys. Rev. B **88**, 054104 (2013).
[35] F. Corsetti, E. Artacho, J. M. Soler, S. S. Alexandre, and M.-V. Fernandez-Serra, J. Chem. Phys. **139**, 194502 (2013).
[36] W. M. C. Foulkes, L. Mitaš, R. J. Needs, and G. Rajagopal, Rev. Mod. Phys. **73**, 33 (2001).
[37] R. J. Needs, M. D. Towler, N. D. Drummond, and P. López-Ríos, J. Phys. Condens. Matter **22**, 023201 (2010).
[38] B. M. Austin, D. Y. Zubarev, and W. A. Lester, Jr., Chem. Rev. **112**, 263 (2012).
[39] A. Y. Wu, E. Whalley, and G. Dolling, Mol. Phys. **47**, 603 (1982).
[40] A. K. Soper and M. A. Ricci, Phys. Rev. Lett. **84**, 2881 (2000).
[41] T. Strässle, A. Saitta, Y. Le Godec, G. Hamel, S. Klotz, J. Loveday, and R. Nelmes, Phys. Rev. Lett. **96**, 067801 (2006).
[42] G. Weck, G. Eggert, P. Loubeyre, N. Desbiens, E. Bourasseau, J.-B. Maillet, M. Mezouar, and M. Hanfland, Phys. Rev. B **80**, 180202(R) (2009).
[43] T. Ikeda, K. Katayama, H. Saitoh, and K. Aoki, J. Chem. Phys. **132**, 121102 (2010).
[44] Y. Katayama, T. Hattori, H. Saitoh, T. Ikeda, and K. Aoki, Phys. Rev. B **81**, 014109 (2010).
[45] V. F. Petrenko and R. W. Whitworth, *Physics of Ice* (Oxford University Press, 1999).
[46] J. Perdew, K. Burke, and M. Ernzerhof, Phys. Rev. Lett. **77**, 3865 (1996).
[47] A. D. Becke, Phys. Rev. A **38**, 3098 (1988); C. Lee, W. Yang, and R. Parr, Phys. Rev. B **37**, 785 (1988).
[48] S. S. Xantheas, J. Chem. Phys. **100**, 7523 (1994).
[49] J. M. Pedulla, F. Vila, and K. D. Jordan, J. Chem. Phys. **105**, 11091 (1996).
[50] A. P. Bartók, M. C. Payne, R. Kondor, and G. Csányi, Phys. Rev. Lett. **104**, 136403 (2010).
[51] I. G. Gurtubay and R. J. Needs, J. Chem. Phys. **127**, 124306 (2007).
[52] F.-F. Wang, M. J. Deible, and K. D. Jordan, J. Phys. Chem. A **117**, 7606 (2013).
[53] T. Helgaker, P. Jorgensen, and J. Olsen, *Molecular Electronic-Structure Theory* (Wiley, 2000).
[54] F. H. Stillinger and A. Rahman, J. Chem. Phys. **61**, 4973 (1974).
[55] R. W. Impey, M. L. Klein, and I. R. McDonald, J. Chem. Phys. **74**, 647 (1981).
[56] G. Jancso, P. Bopp, and K. Heinzinger, Chem. Phys. **85**, 377 (1984).
[57] A. Okhulkov, Y. M. Demaniets, and Y. E. Gorbaty, J. Chem. Phys. **100**, 1578 (1994).
[58] M. C. Bellissent-Funel and L. Bosio, J. Chem. Phys. **102**, 3727 (1995).
[59] E. Schwegler, G. Galli, and F. Gygi, Phys. Rev. Lett. **84**, 2429 (2000).
[60] M. Benoit, M. Bernasconi, P. Focher, and M. Parrinello, Phys. Rev. Lett. **76**, 2934 (1996).
[61] C. Cavazzoni, G. L. Chiarotti, S. Scandolo, E. Tosatti, M. Bernasconi, and M. Parrinello, Science **283**, 44 (1999).
[62] E. Schwegler, G. Galli, F. Gygi, and R. Q. Hood, Phys. Rev. Lett. **87**, 265501 (2001).
[63] A. F. Goncharov, N. Goldman, L. E. Fried, J. C. Crowhurst, I.-F. W. Kuo, C. J. Mundy, and J. M. Zaug, Phys. Rev. Lett. **94**, 125508 (2005).
[64] N. Goldman, L. E. Fried, I.-F. W. Kuo, and C. J. Mundy, Phys. Rev. Lett. **94**, 217801 (2005).
[65] T. R. Mattsson and M. P. Desjarlais, Phys. Rev. Lett. **97**, 017801 (2006).
[66] E. Schwegler, M. Sharma, F. Gygi, and G. Galli, Proc. Natl. Acad. Sci. U.S.A. **105**, 14779 (2008).
[67] M. Boero, K. Terakura, T. Ikeshoji, C. C. Liew, and M. Parrinello, J. Chem. Phys. **115**, 2219 (2001).
[68] F. A. Hamprecht, A. J. Cohen, D. J. Tozer, and N. C. Handy, J. Chem. Phys. **109**, 6264 (1998).
[69] D. Kang, J. Dai, and J. Yuan, J. Chem. Phys. **135**, 024505 (2011).
[70] G. Kresse and J. Furthmüller, Phys. Rev. B **54**, 11169 (1996); see also vasp web-site at www.vasp.at.
[71] P. Blöchl, Phys. Rev. B **50**, 17953 (1994); G. Kresse and D. Joubert, *ibid.* **59**, 1758 (1999).
[72] H. C. Andersen, J. Chem. Phys. **72**, 2384 (1980).
[73] P. Giannozzi *et al.*, J. Phys. Condens. Matter **21**, 395502 (2009).
[74] R. J. Needs, M. D. Towler, N. D. Drummond, and P. López-Ríos, Casino 2.12 User Manual (Cambridge University Press, Cambridge, 2013), see www.tcm.phy.cam.ac.uk/~mdt26/casino.html.
[75] J. R. Trail and R. J. Needs, J. Chem. Phys. **122**, 014112 (2005); J. R. Trail and R. J. Needs, **122**, 174109 (2005).
[76] D. Alfè and M. J. Gillan, Phys. Rev. B **70**, 161101 (2004).
[77] H.-J. Werner, P. J. Knowles, G. Knizia, F. R. Manby, M. Schütz *et al.*, MOLPRO, version 2012.1, a package of *ab initio* programs, 2012, see www.molpro.net.
[78] H.-J. Werner, P. J. Knowles, G. Knizia, F. R. Manby, and M. Schütz, Comput. Mol. Sci. **2**, 242 (2012).
[79] T. H. Dunning, J. Chem. Phys. **90**, 1007 (1989).
[80] R. A. Kendall, T. H. Dunning, and R. J. Harrison, J. Chem. Phys. **96**, 6796 (1992).
[81] G. R. Medders, V. Babin, and F. Paesani, J. Chem. Theory Comput. **9**, 1103 (2013).

[82]V. Babin, G. R. Medders, and F. Paesani, J. Phys. Chem. Lett. **3**, 3765 (2012).
[83]H. Partridge and D. W. Schwenke, J. Chem. Phys. **106**, 4618 (1997).
[84]J. E. Bertie and E. Whalley, J. Chem. Phys. **40**, 1637 (1964); **40**, 1646 (1964).
[85]G. S. Fanourgakis and S. S. Xantheas, J. Chem. Phys. **128**, 074506 (2008).
[86]J. A. Morrone and R. Car, Phys. Rev. Lett. **101**, 017801 (2008).
[87]S. Habershon, T. E. Markland, and D. E. Manolopoulos, J. Chem. Phys. **131**, 024501 (2009).
[88]A. K. Soper, G. W. Neilson, J. E. Enderby, and R. A. Howe, J. Phys. C **10**, 1793 (1977).
[89]A. K. Soper, Phys. Rev. B **72**, 104204 (2005).
[90]H. J. C. Berendsen, J. R. Grigera, and T. P. Straatsma, J. Phys. Chem. **91**, 6269 (1987).
[91]A. K. Soper, J. Phys. Condens. Matter **19**, 335206 (2007).
[92]See supplementary material at http://dx.doi.org/10.1063/1.4885440 for additional data.
[93]A. Luzar and D. Chandler, J. Chem. Phys. **98**, 8160 (1993).
[94]See, e.g., G. N. I. Clark, C. D. Cappa, J. D. Smith, R. J. Saykally, and T. Head-Gordon, Mol. Phys. **108**, 1415 (2010), and references therein.
[95]B. Santra, A. Michaelides, and M. Scheffler, J. Chem. Phys. **131**, 124509 (2009).
[96]M. J. Gillan, D. Alfè, P. J. Bygrave, C. R. Taylor, and F. R. Manby, J. Chem. Phys. **139**, 114101 (2013).
[97]M. Del Ben, M. Schönherr, J. Hutter, and J. VandeVondele, J. Phys. Chem. Lett. **4**, 3753 (2013).
[98]O. A. von Lilienfeld and A. Tkatchenko, J. Chem. Phys. **132**, 234109 (2010).
[99]S. Grimme, J. Comput. Chem. **27**, 1787 (2006).
[100]S. Grimme, J. Antony, S. Ehrlich, and H. Krieg, J. Chem. Phys. **132**, 154104 (2010).
[101]B. M. Axilrod and E. Teller, J. Chem. Phys. **11**, 299 (1943).
[102]A. J. Stone, *The Theory of Intermolecular Forces*, 2nd ed. (Oxford University Press, Oxford, 2013), Sec. 10.2.
[103]D. J. Lacks and R. G. Gordon, Phys. Rev. A **47**, 4681 (1993).
[104]F. O. Kannemann and A. D. Becke, J. Chem. Theory Comput. **5**, 719 (2009).
[105]A. Tkatchenko and O. A. von Lilienfeld, Phys. Rev. B **78**, 045116 (2008).
[106]M. J. Deible, O. Tuguldur, and K. D. Jordan, "Theoretical study of the binding energy of a methane molecule in a $(H_2O)20$ dodecahedral cage," J. Phys. Chem. B (published online) (2014).
[107]M. Schönherr, B. Slater, J. Hutter, and J. VandeVondele, J. Phys. Chem. B **118**, 590 (2014).
[108]QMC benchmark energies for the water clusters treated in the present work are publicly available at http://www.homepages.ucl.ac.uk/~ucfbdxa/qmcwater.htm
[109]A. Tkatchenko, D. Alfè, and K. S. Kim, J. Chem. Theory Comput. **8**, 4317 (2012).
[110]A. Ambrosetti, D. Alfè, R. DiStasio, and A. Tkatchenko, J. Phys. Chem. Lett. **5**, 849 (2014).